A novel Ember Shower Simulator (ESS) for assessing performance of low porosity screens at high wind speeds against firebrand attacks

Ahmad Sharifian, Javad Hashempour[1]

Computational Engineering and Science Research Centre (CESRC),
Faculty of Health, Science and Engineering, University of Southern Queensland,
Toowoomba, Australia

Abstract

Previous studies have shown the effectiveness of low porosity and double layer screens against radiant heat flux from fires. The performance of screens against firebrand attack is also required to be assessed prior to making a decision on their possible application in wildland fire prone areas. The available laboratory-scale devices simulate firebrands at wind speeds less than those of severe firebrand attacks. A relatively low cost, laboratory scale fire ember shower simulator has been designed and manufactured in-house. The simulator is able to assess the performance of low porosity screens at high wind speeds without any reverse flow and possible consequent safety hazards and offers reasonable control over the size and mass of the generated firebrands.

Keywords firebrand generator, ember generator, firebrand shower simulator, ember attack simulator

1. Introduction

Intense wildfires frequently occur in many parts of the world and often cause severe losses in property and human lives. In series of fires in Australia during the Victorian bushfire of 2009, 173 people were killed[1], and the total cost of the damages exceeded 4 billion Australian dollars[2]. The main causes of death and property destruction from wildland fires are radiant heat flux and firebrand attacks mechanism(or spotting), respectively[3,4]. Control of firebrand attacks plays a key role in limiting the progress of wildland fires.

---

[1] Corresponding author, Email: javad.hashempour@usq.edu.au, Tel: +61 (7) 46315322
Computational Engineering and Science Research Centre (CESRC),
Faculty of Health, Science and Engineering, University of Southern Queensland, Toowoomba, Queensland
Australia, QLD 4350.

1   Many codes and regulations developed for construction in wildfire prone areas mandate the

2   use of screens with different apertures for different applications. For example, a standard

3   published by the National Fire Protection Association (NFPA) mandates the coverage of

4   exterior openings of buildings, such as windows, by screens with a maximum aperture size

5   of 6.3 mm [5], the Australian Standard (AS3959-2009) advocates the use of screens with

6   apertures less than 2 mm to cover any openings of houses in bushfire prone areas [6], and the

7   California Residential Code requires openings such as attics and gable vents to be protected

8   by screens with apertures of 1.6 mm to 3.2 mm [7]. Despite these mandatory codes, the

9   literature on the capability of screens to stop firebrand intrusions is sparse. This suggests

10   the need for a review of wildfire construction codes and regulations based on thorough

11   scientific investigation [8].

12   New research requires specialised tools and techniques. For many years, wind tunnels have

13   been used as the main experimental apparatus to study firebrand characteristics. Tarifa et

14   al. [9] investigated the aerodynamic drag and terminal velocity of tethered firebrands of

15   different shapes by igniting and inserting them into a horizontal suction wind tunnel that

16   could provide wind speeds up to 40 m/s. They also designed a vertical wind tunnel with a

17   tapered work section to study the effect of the free motion of firebrands on their burning

18   characteristics. Muraszew et al. [10] also used a horizontal and a vertical wind tunnel to study

19   the ignition and burning characteristics of firebrands in fire whirls. Knight developed a

20   vertical wind tunnel with a tapered work section similar to Tarifa's vertical tunnel to

21   facilitate the study of the aerodynamic and burning characteristics of untethered eucalyptus

22   barks [11]. Ellis found that the combustion characteristics of untethered stringy bark of

23   eucalyptus in the tapered work section of Knight's tunnel was impacted by the non-

24   uniformity of the flow and fragmentation and adherence of the bark to the wall [12]. He

1 improved the uniformity of flow across the test section using a multi-layer screen assembly.

2 Almeida et al. utilised a vertical suction wind tunnel to examine the effect of embers of pine

3 cones and eucalyptus barks' orientation with respect to wind direction and their combustion

4 characteristics at different wind speeds [13]. It is evident that the use of wind tunnels is a

5 valuable approach to study the characteristics of a single firebrand. However, they do not

6 replicate actual firebrand attacks in terms of intensity.

7 A breakthrough was the introduction of a firebrand generator by the National Institute of

8 Standards and Technology - the NIST Dragon [14]. The stand-alone NIST Dragon is capable of

9 producing firebrands of sizes comparable to those of real wildfires. The device consists of a

10 vertical pipe which is connected to a blower at the bottom by a flexible hose. The vertical

11 pipe is formed as two separate parts and the top section is removable from the bottom pipe

12 to allow loading of wood pieces on a fine wire mesh mounted on the top of the lower pipe.

13 The feed (mulch and wood pieces) is ignited with two propane burner torches located in the

14 lower pipe underneath the mesh. The generated firebrands are lifted by blowing air into the

15 upper pipe and finally exiting.

16 A laboratory scale firebrand generator called NIST Baby Dragon also was designed and

17 fabricated, which was coupled with a benchtop wind tunnel used in laboratory scale

18 experiments. Manzello et al. [15,16] carried out experimental studies to investigate firebrand

19 penetration into vents protected by screens in both laboratory and full scale experiments. It

20 is of interest that similar results were reported for both devices. Manzello and Suzuki later

21 added a continuous feed system consisting of a conveyer and feeding gates to the NIST Baby

22 Dragon for non-stop operation and coupled that to the bench scale wind tunnel [17]. The

23 continuous feed system was also added to the full scale NIST firebrand generator and used

24 for full scale experiments on structure vulnerabilities against continuous firebrand attacks

[18]. The design of the NIST firebrand generator was reproduced and used by the Institute for Business and Home Safety (IBHS) in their wind tunnel facility to investigate the performance of building components under firebrand bombardment [19,20]. Their facility contains 105 fans of 1.65 m diameter and five units of the NIST Dragon that are uniformly spaced throughout the test section of 1951 m^2. Each unit of the generator consists of three pipes with different heights of 1.83 m, 3.35 m and 6.40 m, and their installation in the wind tunnel resulted in firebrand showers with wind speeds of up to 58 m/s. In a computational study, the coupling of a firebrand generator inlet to a wind tunnel based on the design of the NIST firebrand generator was investigated[21]. It was found that an optimum mix of firebrand flow and wind tunnel flow can be obtained with the inlet oriented at a 45 degree angle respect to the flow in the wind tunnel.

The size and mass distribution of firebrands in real wildfires have been investigated. Foote et al. determined the size of firebrands generated in the Angora Fire, California, by measuring firebrand-induced melted holes on a trampoline found 9.8 m from an affected house which had a distance of less than 1 mile downwind from the area of crown fire [22]. Analysing the holes on the sheet revealed that more than 85% of the holes had an area less than 50 mm^2. In addition, they inspected 212 locations on or near buildings affected by the fire and reported that the majority of the holes had an area of less than 40 mm^2. Rissel & Ridenour measured firebrand burns (holes) on seven trampoline sheets located on the Bastrop County Complex Fire site in Texas [23]. Measurement of the holes in the trampoline sheets showed that more than 90% of the firebrands had an area of less than 50 mm^2. A field investigation on a prescribed fire in southern New Jersey Pine Barrens, where the vegetation is mainly Pitch Pine, scattered Oaks with understory covered by scrub Oaks, huckle berry and blueberry, discovered that majority of firebrands from barks and shrubs

had a mass in the range of 5 mg to 20 mg[24]. It was also found that the cross-section area of about 80% of the firebrands was less than 20 mm^2.

The size and mass distributions of firebrands generated in laboratory scale experiments have also been investigated. Mass and size distributions of firebrands generated from two Douglas fir trees with heights of 2.6 m and 5.2 m were investigated by Manzello et al.[25]. They reported that 83% of the collected firebrands had a weight of less than 0.3 g and the majority of the firebrands had a surface area of less than 1000 mm^2. They showed that the mass distribution of the firebrands produced from the two trees were similar, with the only difference being that the tallest tree produced heavier firebrands. They had placed water filled pans around the trees to collect the burning firebrands. Later, in another work by Manzello et al.[26], a 4 m high Korean pine was burned in the laboratory and the firebrands were collected by the same method as described for the Douglas fir trees. The measurements showed that 80% of the collected cylindrical-shaped firebrands had a mass of less than 0.3 grams and a majority of them had a surface area of less than 1000 mm^2. Manzello et al. characterised the size of firebrands generated by the NIST Dragon using cylindrical and disk shaped dowels machined from Ponderosa pine trees which are a widespread species in western USA [14]. The cylindrical dowels had diameters from 8 mm to 12.5 mm and lengths of about 50 mm, whereas the disk shape dowels were 25 mm in diameter and 6 mm in length. The generated firebrands were all less than 0.2 g and a vast majority of them had a surface area of less than 1000 mm^2.

A new design of fire ember generator capable of testing low porosity screens at high wind speeds at a relatively small laboratory scale is required. A few computational and experimental studies show that low porosity screens or double layer screens are very effective in lowering the radiant heat flux [27,28,29] and suggest their possible applications as

1   fire barriers. However, their performance against firebrand attacks is also required to be

2   determined if there are plans to deploy them as a fire barrier. The only facility capable of

3   simulating a firebrand attack at full scale and with wind speeds greater than 10 m/s is the

4   IBHS wind tunnel with the cloned NIST firebrand generators. The high wind speed is

5   important because severe firebrand attacks occur at wind speeds of greater than 10 m/s [4,]

6   [30]. The size of the wind tunnel does not appear to be a highly important factor in terms of

7   outcome because the report by Manzello et al. demonstrated similar results from the NIST

8   baby dragon and the NIST full scale Dragon for the experiments with metal screens. This

9   provides an opportunity to use the design of NIST Baby Dragon to reduce the experimental

10   costs. As will be discussed later, the Baby Dragon cannot be coupled to a wind tunnel

11   operating at a high wind speed and/or used for testing low porosity screens due to possible

12   reverse firebrands flow at the inlet of the Baby Dragon (see section 2.1). The fine mesh

13   inside the Baby Dragon pipe considerably reduces the reverse firebrands flow; however,

14   Manzello's study[16] shows that the screens are unable to entirely eliminate firebrand flow

15   which might be a hazard to the operator and equipment.

16   This research aims to design, manufacture and characterise a laboratory scale fire Ember

17   Shower Simulator (ESS) which is able to work in a wider range of wind speeds and to test

18   low porosity screens than those of previously available apparatuses. The design should also

19   be able to produce firebrands with sizes comparable to those of real wildland fires. The

20   following sections describe the design and manufacturing process and present its

21   performance characteristics.

2. Design of ESS

2.1. Limits of current design (NIST baby dragon)

The existing firebrand shower simulator for use at a laboratory scale is the NIST baby dragon or those of similar design. The design consists of a wind tunnel and a firebrand shower generator. The generator includes a separate blower which provides an easy way to regulate the wind speed over the feeds. The blower is the Achilles' heel of the design when it is coupled to a wind tunnel operating at a relatively high wind speed. The authors manufactured a firebrand simulator similar to the Baby Dragon and observed a strong reverse flow that scattered firebrands in the laboratory when a low porosity screen (41%) at a wind speed of 12 m/s was tested. A preliminary computational model of the Baby Dragon showed that the reverse flow is due to the increase of the back pressure before the screen and the problem cannot be avoided by changing the area ratio of the contractor. The reverse flow is the consequence of the pressure built up at the test section under the above described conditions. The built up pressure may exceed the maximum pressure supplied by the blower which, in turn, reverses the flow in the generator.

The limit can be explained by imagining a non-porous sheet with an area equal to that of the test section (a complete blockage, see Figure 1). The blockage causes the flow to be diverted from the wind tunnel to the firebrand generator and then to the outside air. The reverse flow carries the generated firebrands in the generator to the outside and thus is a fire hazard. The combination of extended Bernoulli's, the Darcy Weisbach and, the major and minor loss equations all give the pressure difference between a point before the screen and a point at the exit of the wind tunnel as $k.V^2$ where V is the velocity and K is a coefficient depending on many factors such as the porosity of the screen between the two points. Previous study shows that the pressure loss between the two sides of a screen increases (or

K increases) as the porosity decreases [31]. As the pressure at the exit of the wind tunnel is constant (P_{atm}), the built up pressure behind the screen is the ΔP between these points. The reverse flow slightly lessens if a tiny hole is punched in the sheet (decrease of K). So there are four ways to eliminate the reverse flow at this point. The first is to increase the number of the holes (or decrease of K) which indicates that the design can only operate at porosities higher than a specific value corresponding to the wind speed in the wind tunnel. The second way is to reduce the flowrate in the tunnel to a value equal to or less than the value that can pass through the hole (decrease of V). This demonstrates that the wind speed cannot exceed a certain limit value which depends on the porosity. The third solution is to adjust the blower flow in a way that only stops the reverse flow. This third solution is obviously impractical as it does not provide firebrands in the test section and requires individual adjustment for each experiment. The fourth way is to select a blower that can supply a pressure higher than the built up pressure. This delicate job is also a safety hazard as the flow containing glowing firebrands may reverse back from the inlet of the wind tunnel.

The NIST design can be used in full scale wind tunnels at any wind speed and for all screens regardless of their porosities. The reason is that the firebrand generator is placed inside the full size wind tunnels and therefore its inlet pressure is equal to the built up pressure. As the outlet pressure of the blower is always higher than the inlet pressure, no reverse flow can occur. This is a key element in the design of an ember generator coupled to a benchtop wind tunnel designed to work at high wind speeds and/or with low porosity screens. If the design uses the flow behind the test section as the inlet to the ember generator, it will be a self-adjusting system.

2.2. New design

Figure 2 shows the side and cross-sectional views of the design which was named the Ember Shower Simulator (ESS). The design consists of a wind tunnel including an inlet duct, a contractor and a test section as well as a fire ember generator mounted underneath the tunnel. The fan blows air into the wind tunnel and the air passes through the contractor prior to entering the test section (see Figure 2). In the middle of the contractor, a vertical pipe connects the firebrand generator to the underneath of the tunnel. The vertical pipe is divided into two sections lengthwise by a partition called the splitter to direct a portion of the airflow in the wind tunnel to the ember generator through one half and driving the burning firebrands to the test section in its other half. The splitter also forms a suction region above the exit part of the vertical pipe which helps uplift the firebrands from the generator to the tunnel.

The design does not include a blower to adjust the air speed in the ember generator. However, The ability to control wind speed in the ember generator for both designs is essential because, as a previous study concluded the firebrands produced would be forced out of the generator earlier than planned, resulting in flaming firebrands when the wind speed exceeds a certain value[14]. Therefore the ability to adjust the wind speed in the generator is essential to provide control over the state of combustion. Therefore, the tip of the splitter located in the wind tunnel was designed short, but it can be bolted to flaps with different heights to regulate the amount of air being diverted down and thereby control the wind speed inside the generator. The lofted firebrands mix with the airflow in the wind tunnel which was not diverted down into the ember generator, and then enter the test section prior to exiting the wind tunnel.

The design can still cause a reverse flow when a non-porous sheet is placed in the test section, but it is not a safety concern. In this case, the air from the fan does not enter the tunnel, or only circulates in the inlet section without reaching the ember generator section; therefore the reverse flow does not contain glowing firebrands.

3. Manufacturing of ESS

Figure 3 shows a photograph of the manufactured ESS. The simulator was built in two parts and mounted on a portable stand for ease of transportation and better access to the inside of the tunnel for maintenance and cleaning purposes. An axial fan blows air at an average speed of 5.25 m/s into a square shaped inlet with a cross-sectional area of 1600 cm^2. The fan is mounted on two rails for easy sliding and adjusting the wind speed in the tunnel. The wind tunnel duct is made of a zinc alloy steel sheet with a thickness of 1.3 mm. The lengths of the inlet section and contractor are 1650 mm and 700 mm respectively. The vertical pipe connecting the ember generator into the contractor has a diameter of 150 mm. The splitter is made of a thin zinc alloy coated steel sheet which was welded inside the pipe along its axis. Three flaps with heights of 50 mm, 100 mm and 150 mm were built using the same material as the splitter. The flaps can be bolted to the tip of the splitter and cover the entire width of the contractor at that point (see Figure 3).

The ember generator box is made of a steel sheet with a thickness of 3 mm and its square shaped cross-section is 340 mm long. An access door made of steel was mounted on the front side of the ember generator to place the feeds inside the generator. The feeds to the ember generator can be any type of vegetation. They are ignited by an external ignition source (torch ignitor). After observing a stable flame core, the access door is closed and the fan starts operating. The air diverted into the ember generator not only lofts the generated

firebrands into the wind tunnel but also supplies the required oxygen for combustion. The top of the generator is conical in shape to facilitate the firebrands' passage into the vertical pipe (see Figure 3).

The test section is a square duct with a cross-sectional area of 400 cm^2 and a length of 2000 mm. The top and one side of the test section were made using transparent acrylic sheets for monitoring purposes. In addition, one metre of the top surface of the test section is detachable for mounting screens and cleaning ashes. Screens are slightly stretched and secured by a fixed frame called the screen holder (see Figure 3) at a distance of 800 mm away from the inlet of the test section. The maximum wind speed in the unfilled test section is approximately 21 m/s.

The airflow and firebrands exit the test section at a distance of 1200 mm from the screen. The average wind speed at the exit of the tunnel is measured using a hot wire anemometer. In the case of an emergency which requires an immediate response, municipal water can be sprayed on the fire in the ember generator through a hole in the top of the discharge side of the vertical pipe (see Figure 3). A one-inch (2.54 cm) copper pipe, which is welded to the hole, delivers the municipal water to the hole (see Figure 3).

4. Firebrand quantification

Special software had to be developed to automate the counting of the large number of firebrands and to accurately determine their sizes. The visualisation of the firebrands inside the test section was carried out using a high speed video camera capable of recording images up to 1000 frames per second (fps). It was placed outside the wind tunnel next to the test section to monitor and record the glowing firebrands. Figure 4 shows the glowing

firebrands generated by the ESS on their passage through the test section. The captured

images were then exported to MATLAB for video processing and further analysis.

Since manual counting of such a large number of firebrands is a near impossible task, a

script in the MATLAB environment was developed. The developed script counts the

firebrands within a virtual strip. The width of the strip has a major impact on the accuracy of

the counting. A too narrow or too wide virtual strip could cause no-counting or double-

counting respectively. The width of the strip was initially estimated based on the frame rate

of the camera and assuming an identical speed for firebrands and wind speed. For instance,

for a wind speed of 14.5 m/s and a frame speed of 420 fps, the maximum width of a strip to

avoid double counting should not exceed 35 mm (14500/420). However, firebrand lengths

differ and their speeds are not equal and not necessarily the same as the wind speed. After

comparing the results of the manual and automated counting processes, the best width was

found to be 2 mm, which showed a maximum of 5% difference between the two counting

methods.

A second script was developed to determine the size of firebrands. The photos taken during

the passage of firebrands through the test section show firebrands as seemingly larger than

their actual sizes due to their movement during the camera exposure time. Therefore,

separate photos of the collected firebrands at the exit of the wind tunnel were taken (see

Figure 5a) and were then processed using the second script (see Figure 5b). The script is able

to determine the projected area of the firebrands with a high degree of accuracy depending

on the resolution of the photos.

5. Performance of ESS

Several experiments were carried out to assess the performance of the manufactured ESS. The experiments aimed to assess the proper operation of the system without reverse firebrand flow and to characterize the mass, projected area and mass flux of the generated glowing firebrands as well as the glowing firebrand flux. Three sets of experiments were performed using the flaps of different heights. Each set of experiments was carried out under three wind speeds - low, medium and high - which brought the total number of experiments to nine (see Table 1). An 800 g load of hardwood mulch was fed into the ember generator in the experiments. The feeds had different sizes and masses and were selected from a carefully mixed pile of oven dried hardwood mulch (see Figure 6). The mass and projected (cross-sectional) area of the hardwood mulch varied in the range of 0.04 g to 5 g and 600 mm^2 to 20,000 mm^2.

A wooden L-shaped stand was mounted at the outlet of the tunnel (see Figure 7) to direct the firebrands downward where five water-filled aluminium pans were placed. The water-filled pans technique is the most common technique used in many previous research studies (e.g.[25]). Once the collected wet firebrands were filtered and dried, they were weighed using a 0.0001 g precision scale. The projected area of the firebrands was determined using the script described in the previous section. Most of the recordings lasted 491 seconds due to the memory limitations of the camera at a frame speed of 420 fps with image resolution of 168 x 224 pixels. In a few experiments, the whole process was recorded with lower image resolution of the camera. The combustion of the feed lasted for 10 to 15 minutes depends on the wind speed in the firebrand generator.

The preliminary tests with the ESS indicated that the device works without any reverse flow when metal screens are mounted in the test section. The worst case scenario was a double-

layer screen configuration consisting of two identical screens each with porosity of 41% and aperture size of 0.987 mm. This caused a notable reduction of air speed in the test section due to spillage of air from the gap between the fan and the wind tunnel. However, even in this case, the ESS worked perfectly well without any reverse firebrand flow.

5.1. Velocity Characteristics

An important parameter of the ESS is the air velocity characteristics inside the test section. For this, a hot wire anemometer probe was inserted into the test section at a distance of 150 mm before the screen holder (650 mm after the inlet of the test section). The velocity was recorded at three different heights of 50 mm, 100 mm and 150 mm from the test section floor. The velocity measurements were also performed at the outlet of the test section. The measurements at the outlet were carried out with a 3×3 grid of locations across the section that were equally spaced vertically and horizontally from each other and from the walls. The measurement was repeated several times with and without screens. It was found that the velocity non-uniformity slightly decreases when a screen is used. Therefore, the results presented here are in the absence of a screen which represents the worst case scenario. The measurement was recorded for 420 seconds at a frequency of 1 Hz. The stream wise turbulence intensity was calculated as the root mean square of turbulent velocity fluctuation in stream wise direction (u_{rms}) to the average velocity (u_{ave})[32],

$$T(\%) = \frac{u_{rms}}{u_{ave}} \times 100 \tag{1}$$

The root mean square of fluctuation component (u_{rms}) is calculated as follows,

$$u_{rms} = \sqrt{\frac{1}{n-1} \sum (u_i - u_{ave})^2} \tag{2}$$

Where u_i stands for the instantaneous velocity and n is the number of samples.

Figure 8 indicates instantaneous velocity for the three flaps of 50 mm, 100 mm and 150 mm at two heights of 50 mm and 150 mm. According to Figure 8a, the velocity at the height of 150 mm decreases as a higher flap is used. At the height of 50 mm (Figure 8b), the velocity in the case of the 150 mm flap is the lowest. However, at this height, the velocity in the case of the 100 mm flap is slightly higher than that of the 50 mm flap. This could be explained considering that a higher fraction of the flow in this case has been directed to the ember generator with respect to that of the 50 mm flap. Therefore, for the 100 mm flap and at the height of 50 mm, the effect of the flow from the ember generator is still present even though the average velocity is less than that of the 50 mm flap.

The turbulence intensity at the distance of 150 mm before the screen holder and at the three heights of 50 mm, 100 mm, and 150 mm was calculated based on the measured instantaneous velocities in the absence of a screen. The turbulence intensity increases as the height of the flap increases. The maximum turbulence intensity for the 50 mm flap was measured as 2.4% and increased to 3.7% for the 150 mm flap.

The non uniformity of wind velocity field at the three heights was also quantified at the inlet and outlet of the test section. The velocity and temperature non-uniformity are defined as sample standard deviation (similar to formula 2) divided by the sample mean (similar to formula 1). The non-uniformity of wind velocity field at the three heights was quantified at the inlet and outlet of the test section. The results show that the non uniformity both at the inlet and outlet increases as the flap height increases. At the inlet of the test section, the overall variation of the velocity as the root-mean-square (RMS) percentage of the mean velocity was 2.5% for the 50 mm flap and 9.5% for the 150 mm flap. It should be noted that the maximum non uniformity was 3.5% for the 50 mm flap and 14.2% for the 150 mm flap.

Based on the results at the three flap heights (and each height three points) at the outlet of

1 the test section, the overall variation of the velocity as the root-mean-square percentage of

2 the mean velocity was 6.3% for the 150 mm flap. In this location, the maximum non-

3 uniformity was 10.3%, which shows that the negative impact of flaps on the air flow

4 decreases as the distance between the flap and the location increases.

5 **5.2.   Temperature uniformity**

6 The temperature of the wind flow at the distance of 150 mm before the screen holder and

7 at the three heights was measured. T-type thermocouples were placed at the three heights,

8 and data collection was performed at a sampling frequency of 1 Hz. Figure 9 shows the

9 highest measured temperature non-uniformity which occurred at the lowest velocity setting

10 (corresponding to Figure 8). Similar to the previous section, only the maximum temperature

11 non-uniformities are presented which were obtained when no screen was used. According

12 to the figure, the temperature at all heights increases as flap height increases. For example

13 at the mid-height position, the temperature is 29.1˚C for the 50 mm flap, 32.2˚C for the

14 100 mm flap, and 40.5˚C for the 150 mm flap. This trend was expected as a higher portion of

15 flow is directed to the ember generator when a higher flap is used. The interesting point is

16 that the highest and lowest temperatures occur at the centre and the lowest height (height

17 of 50 mm) of the test section, respectively. For instance, in the case of the 150 mm flap, the

18 temperature was 33.8˚C, 40.5˚C, and 34.4˚C at the heights of 50 mm, 100 mm, and 150 mm

19 respectively. The higher temperature at the height of 150 mm compared to that of the

20 50 mm flap can be speculated upon by the lower density of warm air and the lower

21 conductivity of the acrylic sheets used as the top surface with respect to the zinc alloy steel

22 used for the bottom surface of the test section. The maximum temperature non-uniformity

23 of 4.3˚C was recorded for the 150 mm flap. The maximum temperature non-uniformity

24 decreases to 2.6˚C for the 100 mm flap and to 1.7˚C for the 50 mm flap.

5.3. Firebrands Flow Characteristics

The experimental work shows that the firebrand shower simulator can work with a wide range of porosities and wind speeds without observing any reverse flow jeopardising safety. The lowest porosity tested was double layer identical screens with porosities of 41% (0.987 mm aperture, wire diameter 0.59 mm). The maximum wind speed associated with the different flaps varied and was 18.0 m/s, 14.6 m/s and 10.9 m/s for the flaps with heights of 50 mm, 100 mm and 150 mm respectively. The velocities are the average of nine measurement points at the outlet of the test section (as described in section 5.1).The decrease of velocity with the height of the flap shows it has a substantial contribution to the total loss of energy in the device. Table 1 shows the range of wind speeds observed for each flap by sliding the fan backward or forward. Lower wind speeds than those presented in Table 1 are obtainable by partially blocking the gap between the inlet of the wind tunnel and the fan. Higher wind speeds cannot be generated without utilising a larger or a higher speed fan. The wind speeds were categorised as low, medium and high for each flap in the absence of any screen in the test section, as listed in Table 1.

The flow of firebrands generated by the ESS is not steady, showing random fluctuations on a time scale of several seconds. Therefore, the total numbers of the firebrands at time intervals of one minute were calculated and are presented in Figure 10. The total number of glowing firebrands observed at the test section changed for different amounts of feed placed in the generator but, in all cases, the pattern shown in Figure 10 remained the same. The firebrand flux started from zero, increased to a maximum and eventually fell off back to zero at the end of the experiment. A steadier flow of the firebrands is expected if a continuous feeding system similar to Manzello and Suzuki's studies [17] is integrated with the design.

5.4. *Mass and Projected Area of the Firebrands*

Table 2 lists the average and maximum mass and projected area of the collected firebrands during the nine experiments. According to the table, for a specific flap, increasing the wind speed at the test section increases the size and mass of the generated firebrands. For example, in the case of the 50 mm flap, the average mass and average projected area of the produced firebrands increased from 0.27 mg and 2.59 mm^2 at a wind speed of 13.4 m/s to 1.90 mg and 9.50 mm^2 at a wind speed of 18.0 m/s. The same trend can be observed for the other flaps. Another way to increase the average mass and average projected area of the firebrands is to increase the height of the flap. For instance, the average mass and average projected area increased from 0.79 mg and 4.80 mm^2 for the 100 mm flap at a wind speed of 10.7 m/s to 3 mg and 16.11 mm^2 for the 150 mm flap at a wind speed of 10.9 m/s. The reason for the different average size and mass of the firebrands is believed to be the speed of the wind in the ember generator. A higher wind speed in the wind tunnel or a higher flap causes a higher wind speed in the ember generator which, in turn, carries larger and heavier firebrands into the test section.

Table 3 shows the projected area distribution of the produced firebrands collected from the flow exiting the wind tunnel. The measurements showed that all generated firebrands for the 50 mm flap at the low wind speed (13.4 m/s) had a size less than 50 mm^2. The size of the firebrands increased as the wind speed increased. For example, at wind speeds of 16.0 m/s and 18.0 m/s, 0.1% and 3.3% of the firebrands had an area greater than 50 mm^2 respectively. In the case of the 18.0 m/s wind speed, 0.7% of the firebrands actually had a projected area greater than 100 mm^2. The same pattern was observed for all the flaps utilised in this study. Another way to increase the projected area of the firebrands was to

1   use taller flaps. For instance in the case of the 100 mm flap at a wind speed of 10.7 m/s,

2   99.5% of the firebrands had a size less than 50 mm^2, but this ratio decreased to 93.0% for

3   the 150 mm flap at a wind speed of 10.9 m/s.

4   ***5.5.***   ***Glowing Firebrand Number and Mass Fluxes***

5   The glowing firebrand number flux (or simply firebrand flux) is defined as the number of

6   firebrands passing through the unit area per unit of time. The flux is related to the amount

7   of feed placed in the generator and the wind speed in the firebrand generator, and was not

8   constant throughout any one experiment. However, an average value for each experiment

9   was calculated based on the total number of generated glowing firebrands in the

10   experiment and the overall duration of the experiment (491 s). The average glowing

11   firebrand fluxes of all experiments are displayed in Figure 11a and Table 4.

12   The results show that for the two flaps with the heights of 50 mm and 100 mm, the number

13   of produced firebrands increased with the increase in wind speed. For example in the case

14   of the 50 mm flap, the number flux increases from 378 firebrand/m^{-2}/s^{-1} at the wind speed

15   of 13.4 m/s to 1220 firebrand/m^{-2}/s^{-1} at the wind speed of 18.0 m/s. A similar trend can be

16   observed for the 100 mm flap. However, in the case of the 150 mm flap, the number flux

17   initially increases to a peak and then decreases. This particular case is discussed later (see

18   discussion section below). A photo of the firebrands in this case is presented in Figure 12.

19   The results also showed that the ESS can produce a wide range of firebrand number flux

20   with a maximum of 4415 firebrand/m^{-2}/s^{-1} for an 800 g load of hardwood mulch.

21   An approximate way to calculate the glowing firebrand mass flux is to multiply the firebrand

22   number flux to the average mass of the firebrands for each experiment. The results

23   obtained using this technique should be considered as indicative because the average mass

of glowing firebrands is taken to be equal to the average mass of glowing firebrands that fell into the collecting pans. This was not the case because our observations showed that a smaller percentage of tiny firebrands than that of large firebrands fell into the collecting pans. Consequently, the calculated value tends to be larger than the actual value, particularly for experiments in which large firebrands are produced.

The glowing firebrand mass fluxes were calculated based on the above-mentioned technique and the outcomes are presented in Table 5 and Figure 11b. The results show that the ember generator produces the firebrand mass flux in a wide range from 0.10 $g/m^{-2}/s^{-1}$ to 6.13 $g/m^{-2}/s^{-1}$. According to the results, the mass flux increases by either increasing the wind speed or the height of the flaps.

An important characteristic of the ember generator is the mass ratio of generated glowing firebrands to initial mulch. The total mass of glowing firebrands can be calculated by multiplying the mass flux, the duration of the experiment and the area of the test section. The results are presented in Table 5. According to the results, the total mass of the generated firebrands changed from a minimum of 1.964 g to a maximum of 120.393 g, corresponding to mass ratios of 0.2% and 15.0% respectively. A further experiment is required for a better understanding of the large difference between the minimum and maximum ratios. In a supplementary experiment, a 65.27 g load of the same hardwood mulch used in the previous experiments was completely burned to ashes without allowing the ashes to escape from the container. The final mass decreased to about 2.60 g, representing a decrease of 96%. The results of this experiment are used to illustrate the main results in the discussion section.

6. Discussion

The initial tests of the ESS demonstrate the capability of the design to work under various wind speeds and screen porosities. The reverse firebrand flow was not observed, in spite of using double layer low porosity screens that covered the entire test section. The maximum wind speed in the test section was 21 m/s in the absence of any screen in the test section. The flap causes some turbulence and non uniformity both on temperature and velocity of air flow in the test section. The maximum spatial velocity non uniformity was measured to be 9.54% at the inlet of the test section and 6.34% at the outlet of the test section for the 150 mm flap. The temperature inside the test section reached a steady value after about 2 minutes of the fan running. The maximum temperature non uniformity of 4.7°C was determined at the inlet of the test section for the 150 mm flap. These results call for awareness in the selection of the flap. A high flap produces a higher wind speed in the ember generator as well as higher non uniformities at the test section, which may not be compatible with the requirements of some applications. Generally speaking, a non uniformity greater than 10% is not acceptable, but it reduces to 5% for some applications. In the absence of any information on non uniformity of the Baby Dragon, the 2.5% non uniformity caused by the 50 mm flap appears to be acceptable. A comparison between non uniformities at the inlet and at the outlet of the test section shows that by increasing the distance between the flap and the test section, a better uniformity is achievable. However, this increase may have a negative impact on firebrand flow due to their possible quenching over a longer distance.

The results demonstrated that in the case of the 150 mm flap, contrary to the other cases, the flux of the glowing firebrand at the highest wind speed of 10.9 m/s (2043 Number/m^2/s, see table 4) decreased as compared to that at the medium wind speed of 9.2 m/s (4415

1 Number/m^2/s). This can be explained in two ways. First, from Table 2, it can be seen that

2 the average mass (3.0 mg) and projected area (16.10 mm^2) at the highest wind speed are

3 higher than those (1.3 mg, 7.20 mm^2) at the medium wind speed. This led to the increase in

4 the mass flux, despite the lower number flux (see Figure 11b). An alternative way to explain

5 the decrease of firebrand flux at the highest wind speed is to examine the difference

6 between the estimated total mass of the firebrands in the two cases (Table 5). According to

7 the table, the total mass of the generated firebrands was 120.393 g at the corresponding

8 maximum wind speed and 105.074 g at the medium wind speed. As only negligible amounts

9 of mulch remained in the generator at the end of the experiments, it can be concluded that

10 a higher percentage of firebrands were not properly burned or not burned at all in the case

11 of the maximum wind speed at the 150 mm flap. Figure 12 appears to further support the

12 argument. Therefore, it is reasonable to conclude that for the 150 mm flap, increasing the

13 wind speed in the wind tunnel from medium to high leads to producing a comparatively

14 lower number but larger sized firebrands in the earlier stages of combustion. Therefore, the

15 wind speed in the generator must be limited with short flaps if only the glowing firebrands

16 are required.

17 The supplementary experiment showed that the mulch lost 96% of the initial mass when it

18 was completely burnt. Thus, it was expected that the final mass of the 800 g mulch would

19 become at least 32 g. Table 5 shows that in five out of the nine cases, the final mass was

20 greater than 32 g. This demonstrates that the firebrands were not completely burned.

21 However, in four cases, the final mass of the glowing firebrands were less than 32 g, which

22 shows that a percentage of the firebrands were completely burned before approaching the

23 test section (therefore not counted). It should be noted that observation in these cases

24 ruled out the alternative possibility of unburned firebrands passing through the test section.

Three of the cases were at the low wind speed for the three flaps and the fourth case was for the 50 mm flap at the medium wind speed. These results lead to the conclusion that the wind speed in the generator in these cases was not sufficient to lift heavy firebrands, only the small size or fully burned firebrands and ashes. This demonstrates that the ESS is able to produce a variety of different sizes and masses of firebrands in different stages of combustion.

The results show that the size of the firebrands are slightly smaller than in actual wildfire events. It should be noted that the projected area in this work and the surface area reported in the literature from laboratory studies are not quite the same but the difference does not appear to be significant for the firebrands studied in this work (see Figure 5a). Previous studies revealed that about 85% to 90% of the firebrands produced in actual wildfire events have a size of less than 50 mm^2, which is less than the minimum ratio of 93% measured in this work. This shows that the firebrands produced by the ESS nearly simulate an actual or a slightly worst-case scenario in terms of firebrand penetration through screens.

7. Summary

The study showed that the new fire ember simulator, inspired by the NIST firebrand generator's design, is capable of working with a wide range of wind speeds and testing screens with different porosities without any evidence of reverse flow. The ESS provides some control over the size, mass, number flux and mass flux of firebrands as well as their stages of burning by changing wind speed or adjusting the height of the flaps. The experiments reveal that the average size of the firebrands is slightly less than that of real wildfires. The ESS cannot generate a steady firebrand shower and the flow non-uniformity is

1   perhaps greater than that of the original design. These drawbacks are expected to be

2   eliminated or reduced by the use of a continuous feeding system and by increasing the

3   distance between the test section and the splitter. The ESS requires a more powerful fan for

4   the same wind speed compared to the original design, due to the head loss induced by the

5   splitter and flaps.

1   **NOMENCLATURE**

2   *V*   Velocity

3   *P*   Pressure

        u_{rms} Root mean square of wind velocity

        u_{ave} Average velocity

        u_i Local velocity

        T Turbulence intensity

4

5   **REFERENCES**

6   1.   Cruz, M. G., Sullivan, A. L., Gould, J. S., Sims, N. C., Bannister, A. J., Hollis, J. J. and
7   Hurley, R. J., 2012, "Anatomy of a catastrophic wildfire: The Black Saturday Kilmore
8   East fire in Victoria, Australia," *For. Ecol. Manage.*, **284**, pp. 269–285. DOI:
9   10.1016/j.foreco.2012.02.035

10   2.   Australian Institute of Criminology (AIC), 2009, "Cost of bushfires," Bushfire arson
11   bulletin no. 60 ,Canberra,Australia.

12   3.   Haynes, K., Handmer, J., McAneney, J., Tibbits, A., and Coates, L.,2010, "Australian
13   bushfire fatalities 1900–2008: exploring trends in relation to the 'Prepare, stay and
14   defend or leave early' policy," *Environ. Sci. Policy*, **13**(3), pp. 185–194.
15   DOI:10.1016/j.envsci.2010.03.002

16   4.   Wang, H., 2006, "Ember Attack: Its Role in the Destruction of Houses during ACT
17   Bushfire in 2003," *Australasian Bushfire Conference*, Brisbane, Queensland.

18   5.   National Fire Protection Association, 2008, "NFPA 1144–Standard for protection of
19   life and property from wildfire," Batterymarch Park, MA.

20   6.   Standard Australia, 2009, "Construction of Buildings in Bush Fire Prone Areas (AS
21   3959)," Sydney, Australia.

22   7.   California Residential Code, 2014, "California Code of Regulations Title 24, Part 2.5,"
23   Sacramento, CA.

24   8.   Stephens, S. L., Adams, M., Handmer, J., Kearns, F. R., Leicester, B., Leonard, J. and
25   Moritz, M., 2009, "Urban–wildland fires: how California and other regions of the US
26   can learn from Australia," *Environ. Res. Lett.*, **4**(1), p. 014010.DOI: 10.1088/1748-

9326/4/1/014010

9. Tarifa, C. S., Del Notario, P. P., Moreno, F. G. and Villa, A. R., 1967, "Transport and combustion of firebrands," *U.S. Dep. Agric. For. Serv.*, vol. II.

10. Muraszew, A., Fedele, J. B. and Kuby, W. C., 1977, "Trajectory of firebrands in and out of fire whirls," *Combust. Flame*, **30**, pp. 321–324,DOI: 10.1016/0010-2180(77)90081-5.

11. Knight, I., 2001, "The design and construction of a vertical wind tunnel for the study of untethered firebrands in flight," *Fire Technol.*,**37**(1) pp. 87–100.DOI: 10.1023/A:1011605719943

12. Ellis, P. F. M., 2013, "Firebrand characteristics of the stringy bark of messmate (Eucalyptus obliqua) investigated using non-tethered samples," *Int. J. Wildl. fire*, **22**(5), pp. 642–651.DOI: 10.1071/WF12141

13. Almeida, M., Viegas, D. X., Miranda, A. I. and Reva, V., 2009, "Combustibility of potential embers," in *18th World IMACS/MODSIM Congress*, pp. 4388–4394.

14. Manzello, S. L., Shields, J. R., Cleary, T. G., Maranghides, A., Mell, W. E., Yang, J. C., Hayashi, Y., Nii, D. and Kurita, T., 2008, "On the development and characterization of a firebrand generator," *Fire Saf. J.*, **43**, pp. 258–268.DOI: 10.1016/j.firesaf.2007.10.001

15. Manzello, S. L., Park, S.-H., Shields, J. R., Hayashi, Y. and Suzuki, S., 2010, "Comparison Testing Protocol for Firebrand Penetration through Building Vents : Summary of BRI" NIST Full Scale and NIST Reduced Scale Results NIST Technical Note 1659, National Institute of Standard and Technology.

16. Manzello, S. L., Park, S.-H., Suzuki, S., Shields, J. R. and Hayashi, Y., 2011, "Experimental investigation of structure vulnerabilities to firebrand showers," *Fire Saf. J.*, **46**(8), pp. 568–578.DOI: 10.1016/j.firesaf.2011.09.003

17. Manzello, S. L. and Suzuki, S., 2012, "The new and improved NIST Dragon's LAIR (Lofting and Ignition Research) facility," *Fire Mater.*, **36**(8), pp. 623–635.DOI: 10.1002/fam.1123

18. Manzello, S. L. and Suzuki, S., 2013,"Experimentally Simulating Wind Driven Firebrand Showers in Wildland-urban Interface (WUI) Fires: Overview of the NIST Firebrand Generator (NIST Dragon) Technology," *Procedia Eng.*, **62**, pp. 91–102. DOI: 10.1016/j.proeng.2013.08.047

19. Quarles, S. and Sindelar, M., 2011, "Wildfire ignition resistant home design (WIRHD) program: Full-scale testing and demonstration final report," No. 11-14-R. USDA Forest Service-Savannah River, New Ellenton, SC.

20. Quarles, S., 2012, "Vulnerabilities of Buildings to Wildfire Exposures," *extension*. [Online]. Available: http://www.extension.org/pages/63495/vulnerabilities-of-

1   buildings-to-wildfire-exposures#.VPeXW_mUeQB.

2   21.   Hashempour, J. and Sharifian, A., 2013, "Optimizing the Coupling of a Firebrand
3   Generator to a Horizontal Wind Tunnel," *Adv. Mater. Res.*, **726–731**, pp. 971–
4   976.DOI: 10.4028/www.scientific.net/AMR.726-731.971

5   22.   Foote, E., Liu, J. and Manzello, S., 2011, "Characterizing firebrand exposure during
6   wildland urban interface fires," in *Proceedings of Fire and Materials*, pp. 1–12.

7   23.   Rissel, S. and Ridenour, K., 2013, "Ember production during the Bastrop complex
8   fire," *Fire Manag.*, **7**.

9   24.   El Houssami, M., Mueller, E., Filkov, A., Thomas, J. C., Skowronski, N., Gallagher, M.
10   R., Clark, K., Kremens, R. and Simeoni, A., 2015, "Experimental Procedures
11   Characterising Firebrand Generation in Wildland Fires," *Fire Technology,* pp.1-21.DOI:
12   10.1007/s10694-015-0492-z

13   25.   Manzello, S. L., Maranghides, A. and Mell, W. E., "Firebrand generation from burning
14   vegetation," *Int. J. Wildl. Fire*, **16**, pp. 458–462, 2007.DOI: 10.1071/WF06079

15   26.   Manzello, S. L., Maranghides, A., Shields, J. R., Mell, W. E., Hayashi, Y. and Nii, D.,
16   2009, "Mass and size distribution of firebrands generated from burning Korean pine
17   (Pinus koraiensis) trees," *Fire Mater.*, **33**(1), pp. 21–31. DOI: 10.1002/fam.977

18   27.   Sharifian, A. and Buttsworth, D., 2008,"Direct radiation from wildfires through square
19   woven screens," in *ASME Summer Heat Transfer*.DOI: 10.1115/HT2008-56270

20   28.   Sharifian, A. and Buttsworth, D., 2010, "Double-layered metal mesh screens to
21   contain or exclude thermal radiation from bush fires," *J. Fire Prot. Eng.*, **20**(4), pp.
22   291–311.DOI: 10.1177/1042391510367366

23   29.   Hashempour, J., Sharifian, A. and Billingsley, J., 2016, "An experimental approach to
24   measure direct radiation through single-layer square cell plain woven screens," *ASME
25   J. Heat Transf.*, 138(1), pp. 012701–012706.DOI: 10.1115/1.4031110

26   30.   Chen, K., 2004, "Quantifying bushfire penetration into urban areas in Australia,"
27   *Geophys. Res. Lett.*, **31**(12), p. L12212.DOI: 10.1029/2004GL020244

28   31.   Sharifian, A. and Buttsworth, 2007 "Computational Simulation of the Wind-force on
29   Metal Meshes," in *16th Australasian Fluid Mechanics Conference*, December, pp. 2–6.

30   32.   Cebeci, T., 1974, *Analysis of turbulent boundary layers*, Academic Press INC.,London,
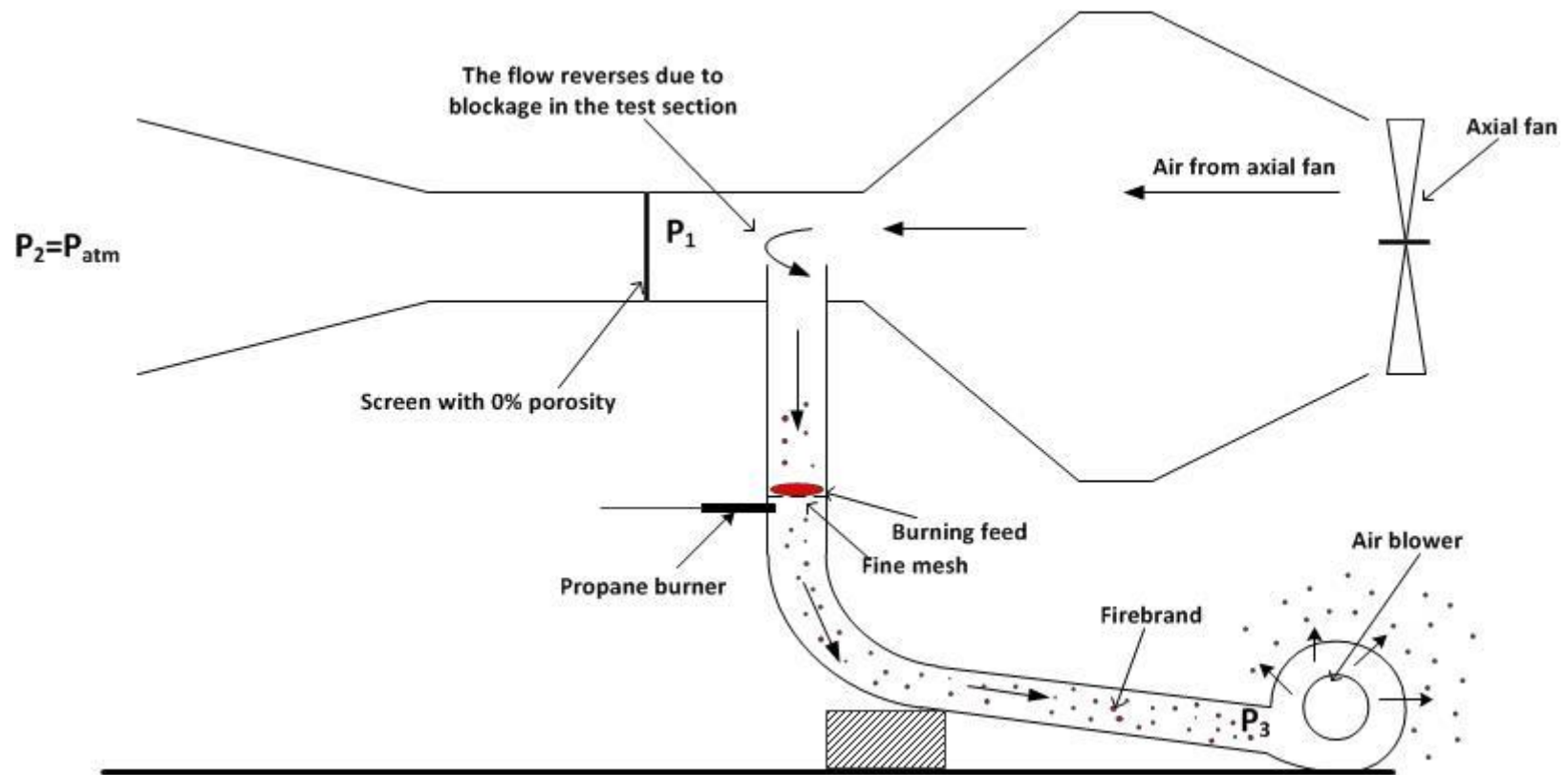31   UK, ISBN 0-12-164650-5.
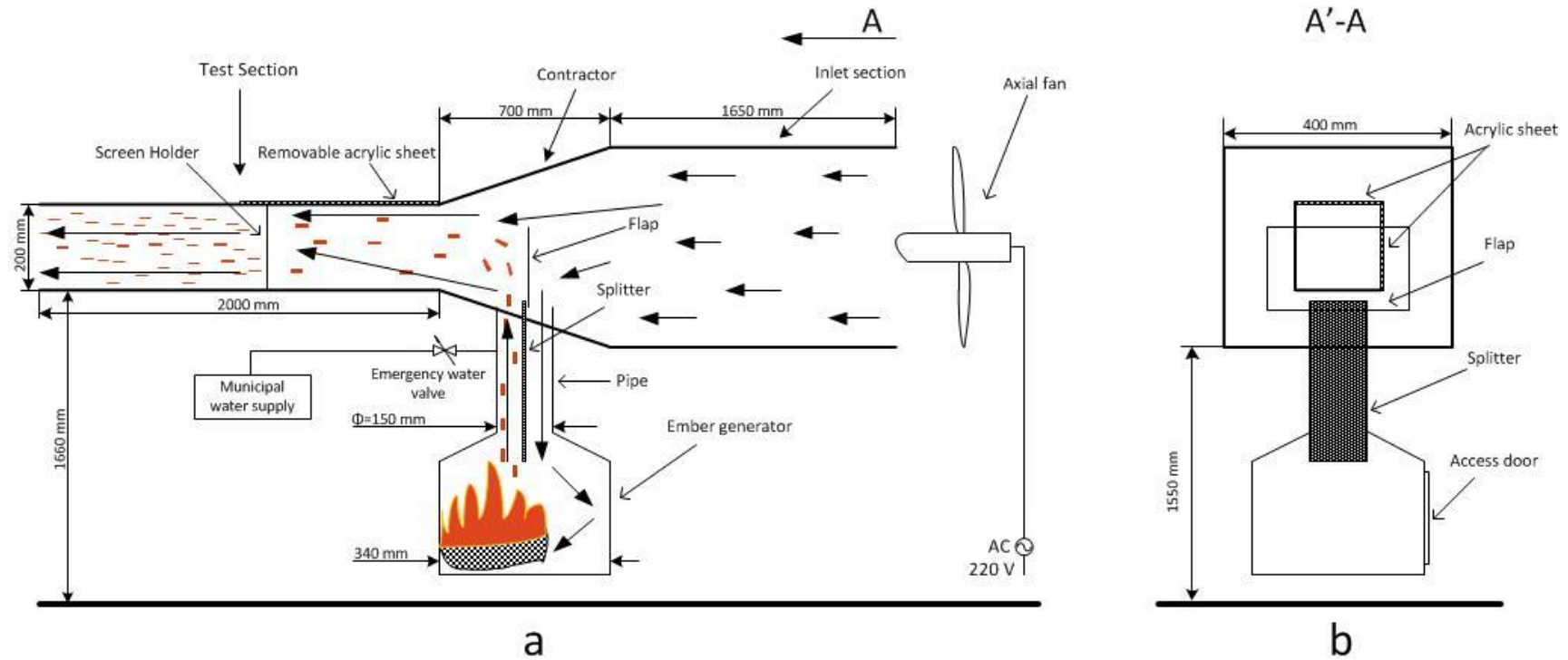
32

Figure 1 Scheme of reverse flow in NIST baby dragon.

Figure 2 Scheme of the Ember Shower Simulator (ESS): a) side view; b) cross-section view.
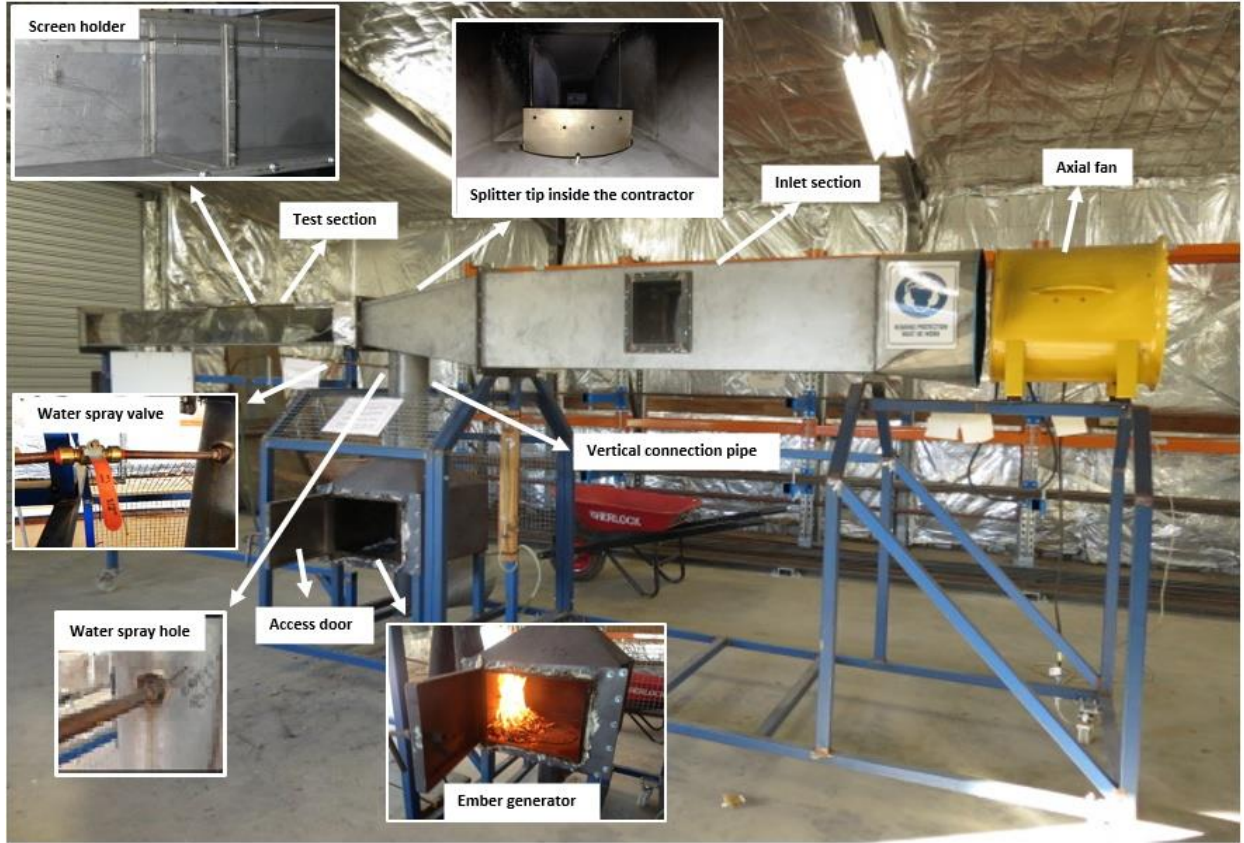
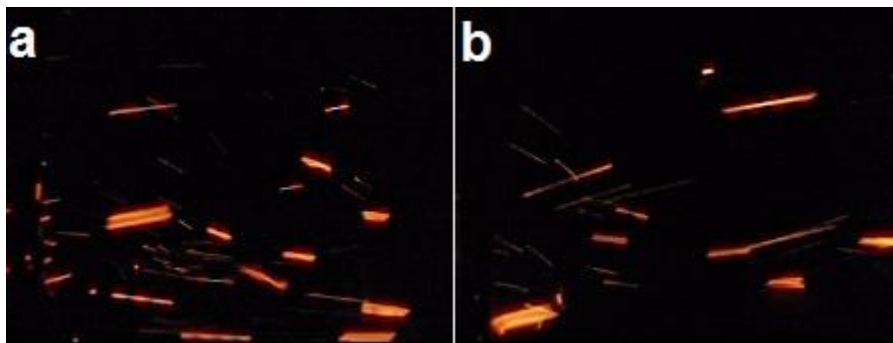*Figure 3 Photographs of the Ember Shower Simulator (ESS).*

Figure 4 Firebrands produced at: a) wind speed of 14.7 m/s and flap height of 100 mm; b) wind speed of 18 m/s and flap height of 50 mm.
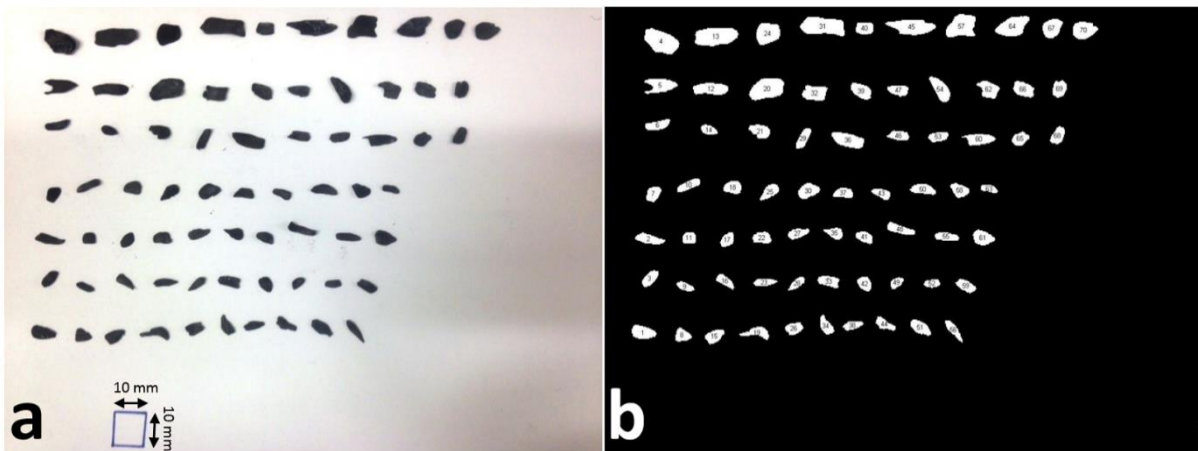
Figure 5 Image of collected firebrands in experiments with flap of 100 mm and wind speed of 10.7 m/s: a) actual photo; b) binary image.

Figure 6 Hardwood mulch applied as feed in generator: a) 800 g hardwood mulch; b) hardwood mulch in the generator.
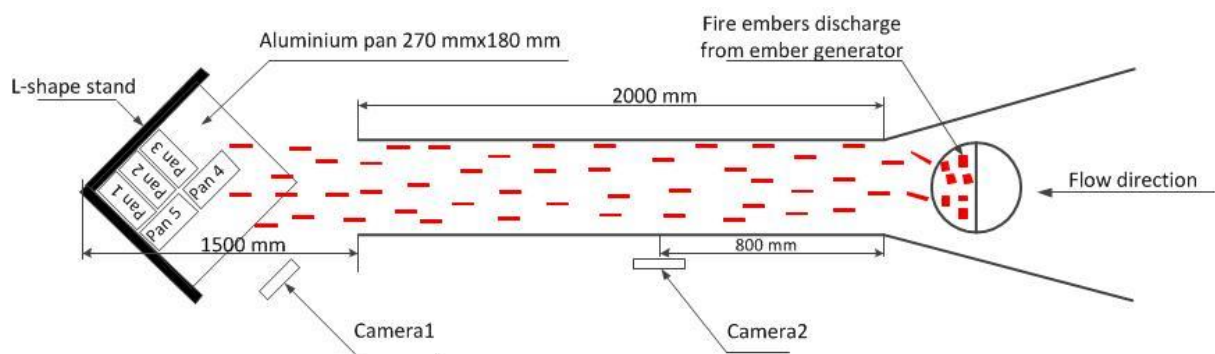
Figure 7 Top view of experiment layout for collecting glowing firebrands generated by the ESS.
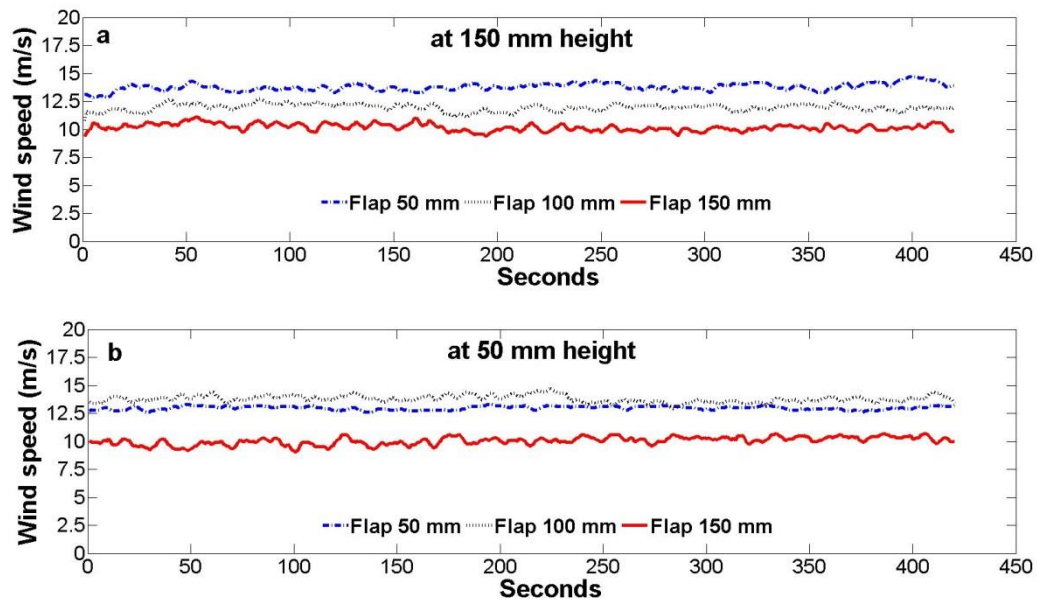
Figure 8 the instantaneous velocity distribution inside the unfilled test section measured at lowest velocity setting for the applied flaps a) at 150 mm height from the tunnel floor b) at 50 mm height from the tunnel floor.
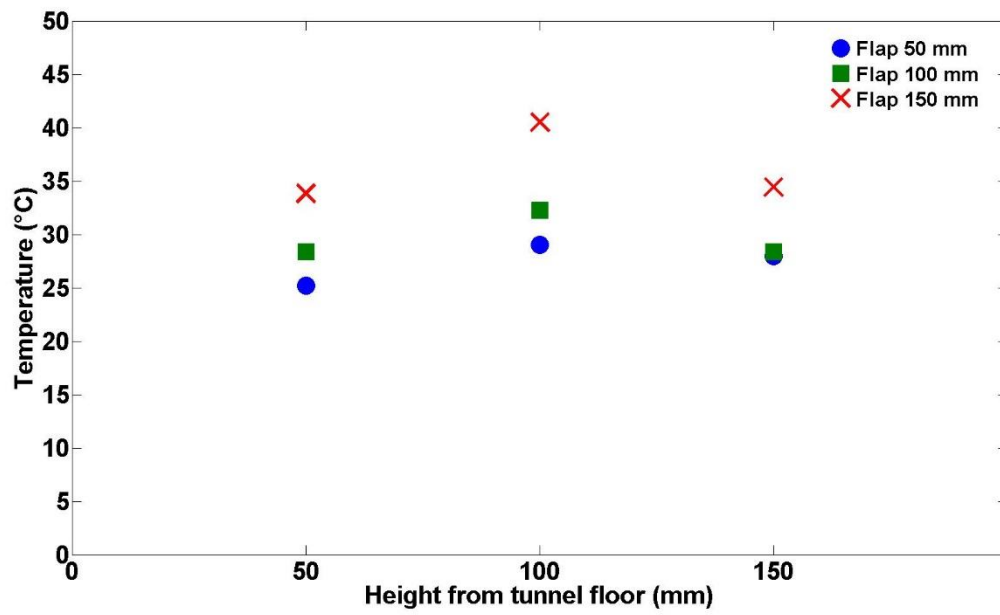
Figure 9 Temperatures profile inside the test section at room temperature of 19°C for the three flaps of 50 mm, 100 mm and 150 mm.
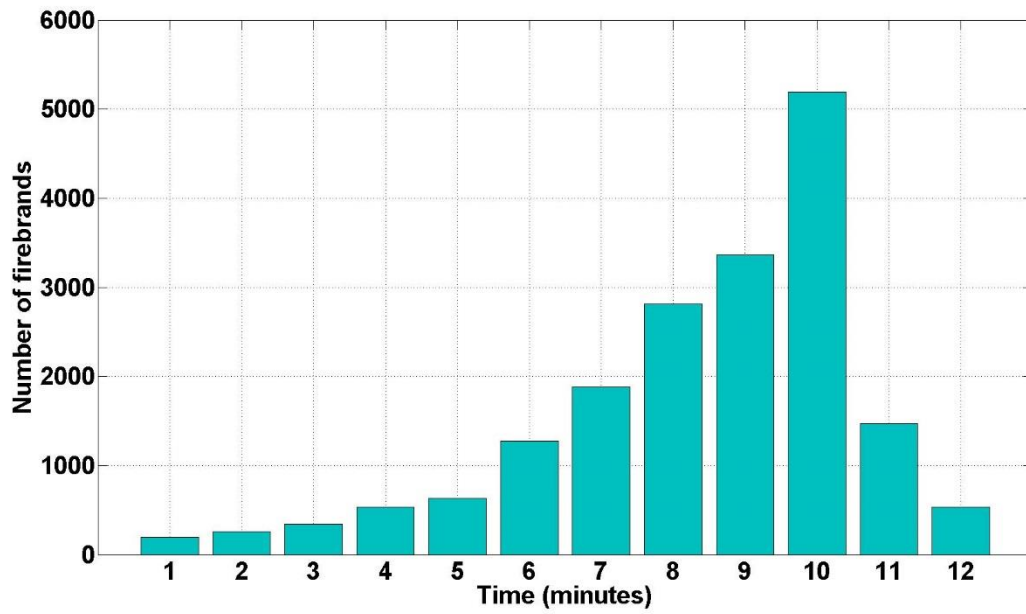
Figure 10 Number flux of firebrands generated by the ESS with wind speed of 16 m/s at the test section and flap height of 50 mm.
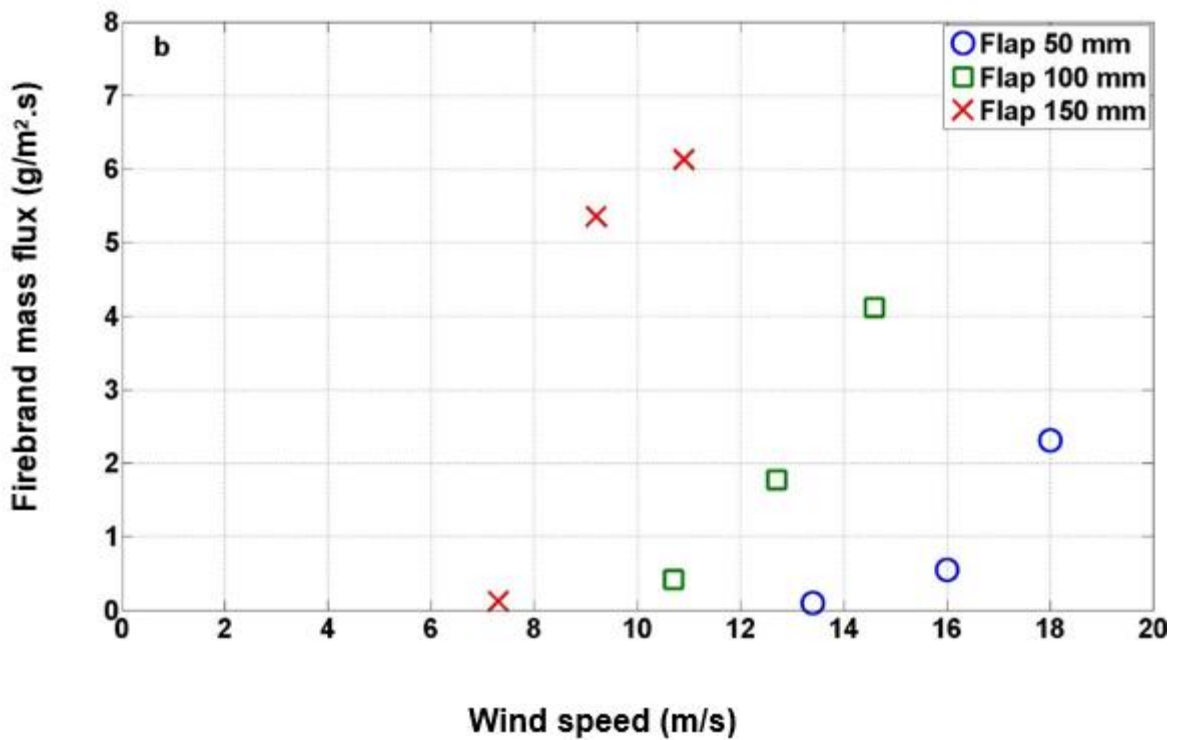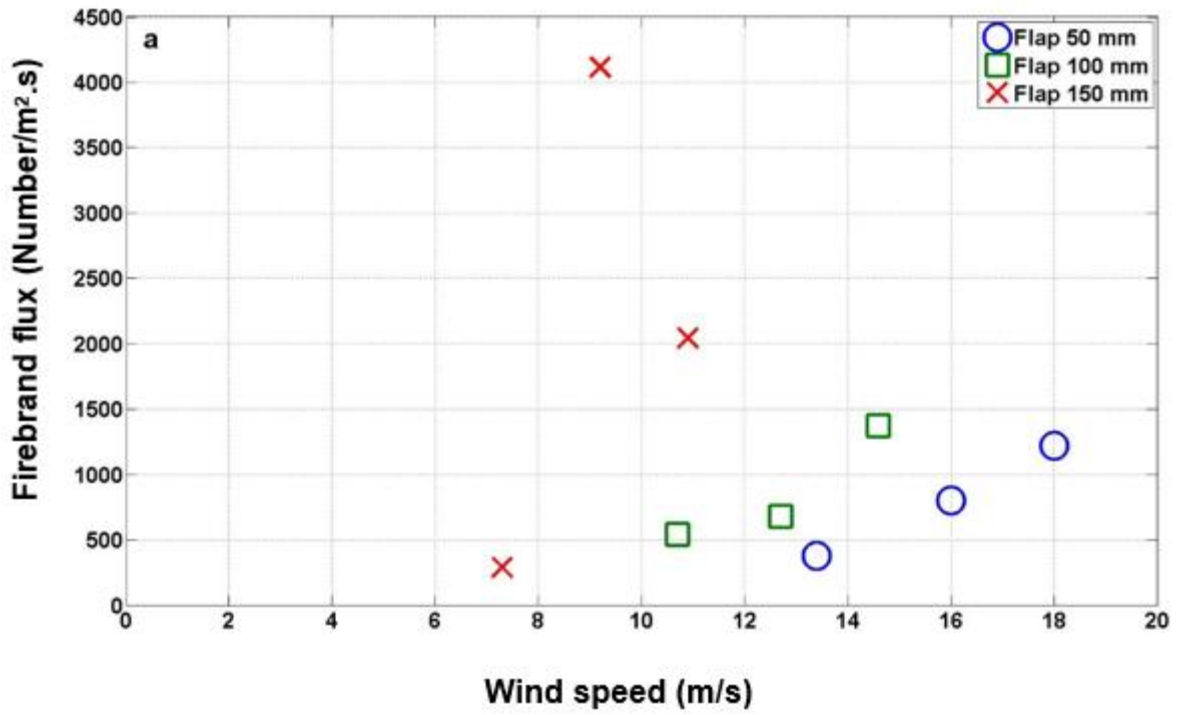
Figure 11 a) Number flux of collected firebrands at different flaps versus wind speeds at the test section; b) Mass flux of collected firebrands at different flaps versus wind speeds at the test section

Figure 2 Collected firebrands in experiment with flap of 150 mm and high wind speed.

Table 1 Range of wind speeds at the test section of the ESS for different flaps.

Flap Height (mm)	Wind Speeds (m/s)		
	Low	*Medium*	*High*
50	13.4	16.0	18.0
100	10.7	12.7	14.6
150	7.3	9.2	10.9

Table 2 Mean and maximum of mass and projected area of collected firebrands in different experiments with different flaps and wind speeds at the test section

Flap Height (mm)	Wind speed (m/s)	Mass (milligrams)		Projected area (mm²)	
		average	*maximum*	*average*	*maximum*
50	13.4	0.27	6.7	2.60	36.6
	16.0	0.69	15.6	4.90	82.8
	18.0	1.90	44.4	9.50	161.2
100	10.7	0.79	17.0	4.80	70.3
	12.7	2.60	57.2	12.70	240.3
	14.6	3.00	118.0	13.70	197.7
150	7.3	0.40	13.0	2.60	105.5
	9.2	1.30	23.4	7.20	137.6
	10.9	3.00	62.1	16.10	259.0

Table 3 Firebrand size distribution collected at the exit of the wind tunnel in experiments with different flaps and wind speeds at the test section.

Projected area, A_p (mm^2)	Firebrand size distribution (%)								
	Flap 50 mm			Flap 100 mm			Flap 150 mm		
	13.4 (m/s)	16.0 (m/s)	18.0 (m/s)	10.7 (m/s)	12.7 (m/s)	14.6 (m/s)	7.3 (m/s)	9.2 (m/s)	10.9 (m/s)
Ap<50	100.0%	99.9%	96.7%	99.5%	96.1%	93.9%	99.9%	98.2%	93.0%
50 <Ap< 100	0.0%	0.1%	2.6%	0.5%	3.2%	4.9%	0.0%	1.5%	5.5%
Ap >100	0.0%	0.0%	0.7%	0.0%	0.7%	1.2%	0.1%	0.3%	1.5%

Table 4 Number and mass fluxes of firebrands in different experiments with different flaps and wind speeds at the test section.

Glowing firebrands	Flap 50 mm			Flap 100 mm			Flap 150 mm		
	13.4 (m/s)	16.0 (m/s)	18.0 (m/s)	10.7 (m/s)	12.7 (m/s)	14.6 (m/s)	7.3 (m/s)	9.2 (m/s)	10.9 (m/s)
Number flux (Number/m^2/s)	378	804	1220	540	681	1374	288	4415	2043
mass flux (g/m^2/s)	0.10	0.55	2.31	0.42	1.77	4.12	0.12	5.35	6.13

Table 5 Total estimated of generated firebrands in experiments with different flaps and wind speeds at the test section.

Flap height (mm)	Wind speed (m/s)	Mass of generated glowing firebrands (grams)
50	13.4	1.964
	16.0	10.802
	18.0	45.369
100	10.7	8.249
	12.7	34.763
	14.6	80.917
150	7.3	2.357
	9.2	105.074
	10.9	120.393